Sensors International 6 (2025) 100332

Contents lists available at ScienceDirect

Sensors International

journal homepage: www.keaipublishing.com/en/journals/sensors-international

Development of a sugar-derived silver nanoparticle-based electrochemical immunosensor for sensitive D-dimer detection

Fatma Ozturk Kirbay [a,b,*], İdris Yazgan [b], Dilek Odaci [a]

[a] Department of Biochemistry, Faculty of Science, Ege University, 35100, İzmir, Turkiye
[b] Center for Biosensors and Material Science, Faculty of Science of Kastamonu University, 37100, Kastamonu, Türkiye

ARTICLE INFO

Keywords:
Immunosensor
Biomarker
D-dimer
Electrodeposition
Silver nanoparticle

ABSTRACT

D-dimer (DD) is a key marker of coagulation and fibrinolysis activation. Clinicians can make important decisions with the aid of quick analysis and quantification, ideally at the patient's bedside. Electrochemical immunosensors are effective point-of-care technologies to address these issues. Here, we describe the development of a simple electrochemical immunosensor to detect DD. The immunosensor is constructed by electrodeposition of lactose methoxide aniline silver nanoparticles (LMA-AgNPs) on a screen-printed carbon electrode (SPCE). The LMA-AgNP and SPCE/LMA-AgNP were characterized by Fourier transform infrared (FTIR) spectroscopy, high-resolution transmission electron microscopy (HR-TEM), scanning electron microscopy-energy dispersive X-ray spectroscopy (SEM-EDS), and X-ray photoelectron spectroscopy (XPS). The electrochemical behavior of the SPCE/LMA-AgNP was examined using electrochemical impedance spectroscopy (EIS), differential pulse voltammetry (DPV), and cyclic voltammetry (CV). Then, Anti-D-Dimer antibody (Anti-DD) was immobilized on SPCE/LMA-AgNP. Along with the analytical characterization of the SPCE/LMA-AgNP/Anti-DD immunosensor, the linear range for DD, limit of detection (LOD), potential chemical interferences, and real sample applications were also evaluated. The antigen/antibody interaction at various DD concentrations was monitored using DPV. The SPCE/LMA-AgNP/Anti-DD shows a linear response in the DD concentration range of 0.01–1 pg/mL and a LOD of 0.2 fg/mL. In addition, the SPCE/LMA-AgNP/Anti-DD showed excellent specificity and no response to potential interfering substances, for instance urea, insulin, C-reactive protein (CRP), and serum amyloid A (SAA). Eventually, the SPCE/LMA-AgNP/Anti-DD is applied in human serum, which shows good recovery values (97.2 %). The SPCE/LMA-AgNP/Anti-DD can be fabricated cheaply and easily for bedside clinical evaluation.

1. Introduction

D-dimer (DD) is a sensitive marker of coagulation and fibrinolysis activation, making it particularly valuable as a biomarker for intravascular thrombosis. Elevated blood levels of DD have been found to be strongly associated with the incidence of cancer-related thrombosis, pulmonary embolism (PE), disseminated intravascular coagulation (DIC), deep vein thrombosis (DVT), venous thromboembolism (VTE), and stroke. Patients with malignancies of the lung [1], breast [2], lower gastrointestinal tract [3], pancreatic, stomach, kidney, prostate, and brain are also at higher risk of dying if their DD levels are elevated. Recently, DD has also been identified as a key biomarker for assessing the prognosis of COVID-19 [4]. Therefore, rapid and portable DD tests are welcomed by physicians since they could potentially save lives by enabling immediate results in emergency medical vehicles.

Clinical labs employ a number of methods to measure DD levels, including immunoturbidimetry, latex agglutination, chemiluminescence, immunofluorescence, and enzyme-linked immunosorbent assay (ELISA). DD is expressed in fibrinogen equivalent units (μg/mL) [5–7]. These methods provide high-throughput analysis with satisfactory accuracy and have become the standard for routine DD testing. However, they still require response times in excess of several minutes. Because they combine high sensitivity, selectivity, and quick reaction times (within a few minutes), biosensors have become highly effective tools for biomarker identification in this setting.

In the previous decades, various nanomaterials have been used in the development of electrochemical sensors to improve their analytical performance. The integration of nanoscale materials into the biosensor

Peer review under the responsibility of KeAi Communications Co., Ltd.
* Corresponding author. Department of Biochemistry, Faculty of Science, Ege University, 35100, İzmir, Turkiye
E-mail address: ffatma.ozturkk@gmail.com (F.O. Kirbay).

https://doi.org/10.1016/j.sintl.2025.100332
Received 26 December 2024; Received in revised form 6 March 2025; Accepted 27 March 2025
Available online 28 March 2025

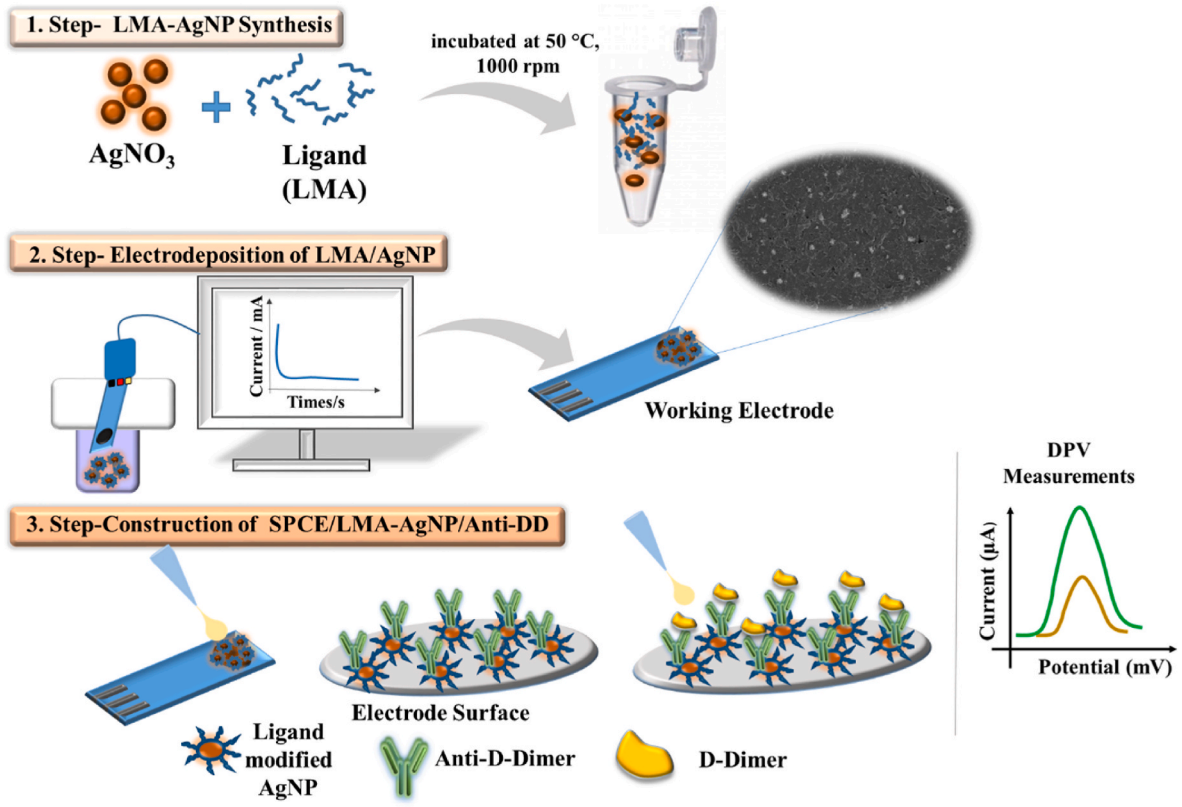

Scheme 1. Schematic illustration of the developed immunosensor platform step by step.

platform significantly enhances the sensitivity of the biosensor by allowing the immobilization of a greater number of bioreceptors and, in some cases, enabling the nanomaterials themselves to act as transduction elements [8]. The most often utilized nanomaterials in the creation of biosensors for DD detection are graphene [12], carbon nanotubes [10,11], and gold nanoparticles [9]. Alternatively, because of their remarkable physicochemical characteristics, silver nanoparticles (AgNPs) have become one of the most well-known and extensively utilized materials for the development of flexible electrochemical sensing platforms [13]. The sensitivity and stability of the sensor platform are closely related to the proper dispersion of the AgNPs and the prevention of their aggregation within the network or matrices. Stabilization of AgNPs is achieved by steric and electrostatic repulsion mechanisms facilitated by stabilizing agents such as polymers or other matrix materials [14]. Yazgan et al. (2020) presented a study demonstrating a novel approach using sugar derivatives as reducing, stabilizing, and capping agents for the synthesis of gold (Au) and silver (Ag) nanostructures [15], which can be combined with polymers (e.g. cellulosic polymers) [16]. Therefore, in this study, we synthesized lactose methoxide aniline (LMA) to synthesize shape- and size-controlled Ag nanostructures, eliminating the need for additional reducing, shape-directing, or stabilizing agents.

Here, the electrochemical behaviors of the developed sugar derivative AgNPs and their potential use for the preparation of immunosensor were compared. LMA-AgNPs were synthesized, electrodeposited on a SPCE and the formed the SPCE/LMA-AgNP was used as an Anti-D-dimer antibody (Anti-DD) immobilization matrix. Firstly, LMA-AgNPs were electrodeposited onto a SPCE used as a working electrode. LMA-AgNPs and the SPCE/LMA-AgNP were characterized by Fourier transform infrared (FTIR) spectroscopy, high-resolution transmission electron microscopy (HRTEM), scanning electron microscopy-energy dispersive X-ray spectroscopy (SEM-EDS), and X-ray photoelectron spectroscopy (XPS). Covalent conjugation of Anti-DD on SPCE/LMA-AgNP was performed using N-(3-dimethylaminopropyl)-N′-ethylcarbodiimide hydrochloride/N-hydroxysuccinimide (EDC/NHS) to create SPCE/LMA-AgNP/Anti-DD biofunctional surface. In the presence of DD, electrochemical measurements were performed on SPCE/LMA-AgNP/Anti-DD using DPV, CV, and EIS techniques. As a result, the proposed SPCE/LMA-AgNP/Anti-DD showed good linear range, low limit of detection (LOD), good repeatability, no substance interference, and sample application was carried out successfully to detect DD in human serum.

2. Material and methods

2.1. Materials

Lactose, potassium hexacyanoferrate $K_3[Fe(CN)_6]$, monosodium phosphate (NaH_2PO_4), and potassium chloride (KCl), N-(3-dimethylaminopropyl)- N′ -ethylcarbodiimide hydrochloride (EDC), and N-hydroxysuccinimide (NHS) were purchased from Sigma-Aldrich. Human D-Dimer and mouse anti-Human D-Dimer were from Bio-Rad. Screen-printed carbon electrodes (SPCE) were from Methrom. Britton-Robinson buffer was prepared by mixing 0.04 M boric acid, 0.04 M phosphoric acid, and 0.04 M acetic acid and adjusting to the desired pH with 0.2 M NaOH. Lactose methoxyaniline was synthesized in our labs as described in the literature [15,17].

2.2. Equipments

PalmSens recorded the electrochemical measurements. The modified and unmodified SPCE surfaces were characterized by SEM (Zeiss, Sigma 300), which underwent gold coating using a Leica EM ACE600 before SEM. The morphological characterization of the Ag nanoparticles was performed by HRTEM (FEI TALOS F200S TEM 200 kV). The SPCE/LMA-AgNP and SPCE/LMA-AgNP/Anti-DD were investigated by XPS, which was performed using a Thermo Scientific Model K-Alpha XPS apparatus, using monochromatic Al Ka radiation with an energy of 1486.7 electron volts (eV). UV–Vis absorption spectra of LMA-AgNP was recorded using

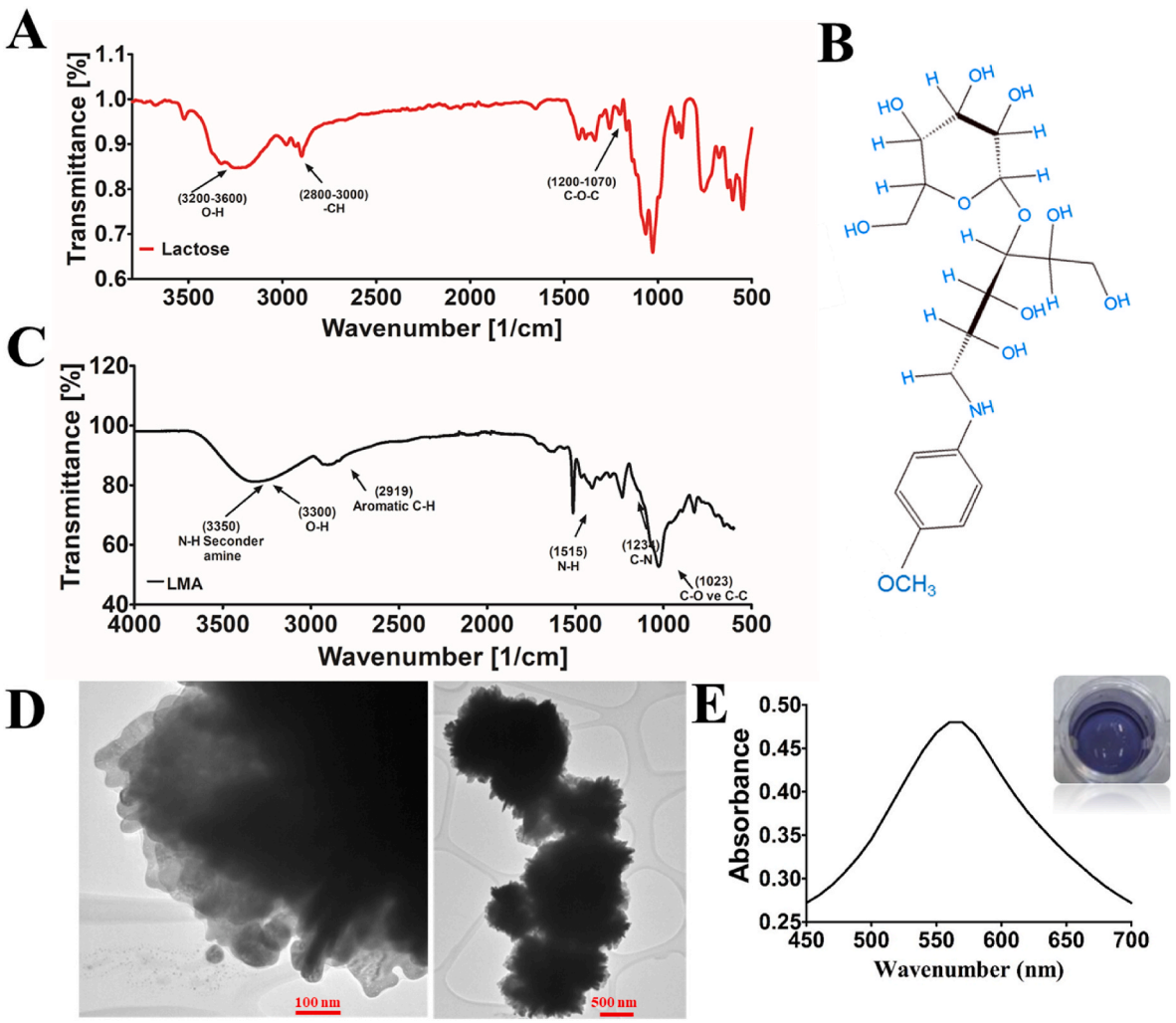

Fig. 1. FT-IR spectrums of A) Lactose C) LMA, B) molecular structure of synthesized LMA sugar ligand D) TEM micrographs of LMA-AgNP, and E) UV–Vis spectrum of LMA-AgNP.

a UV–Vis microplate spectrophotometer (Biotek, Winooski, VT, USA).

2.3. Construction of sensor platform and electrochemical measurements

Previously, we showed that sugar ligands can serve as reducing, capping, and stabilizing agents in AgNPs synthesis [16,18]. Briefly, solution of 100 mg/mL LMA was mixed with 100 mg/mL $AgNO_3$ in distilled water at a 20:1 (v:v) ratio. The mixture was incubated at 50 °C for 1 h under stirring at 1000 rpm. Utilization of the LMA contains seconder amino group that was needed to immobilize Anti-DD on the electrode surface through EDC/NHS chemistry. It should be mentioned that the preparation of LMA-AgNPs helped us to form amine groups on the electrode surface for loading higher amounts of Anti-DD and uniform AgNPs.

LMA-AgNPs-modified SPCE has been used as a working electrode in electrochemical measurements. This paper describes a simple method for obtaining AgNPs -modified SPCE. The method involves the electrochemical deposition of AgNPs onto the working electrode surface using an LMA-AgNP solution in Britton-Robinson buffer (pH 2). Electrodeposition was achieved by applying an accumulation potential for a specified time with constant stirring [19]. Therefore, pH 2 Britton-Robinson buffer solution was used during the deposition step because AgNPs require a highly acidic environment during the deposition on the carbon electrode. In addition, long deposition times or highly negative potentials are required for effective AgNPs deposition. Therefore, we selected conditions of −1.20 V and 120 s for the deposition process. Previous experiments have shown that highly acidic pH values are required to deposit AgNPs on the carbon surface of the electrode. Therefore, a Britton-Robinson solution at pH 2 was used during deposition [20–22].

EDC/NHS chemistry was utilized to conjugate Anti-DD onto the SPCE/LMA-AgNP surface. A solution comprising 20 μg/mL Anti-DD, 12.5 mM NHS, and 50 mM EDC in pH 7.4 PBS was preincubated for 15 min at 1000 rpm. Subsequently, 5 μL of this mixture was applied to the SPCE/LMA-AgNP surface and left to dry, which required approximately 2h. After rinsing the surface with distilled water to eliminate any unbound Anti-DD, the sensing surface (SPCE/LMA-AgNP/Anti-DD) was ready for DD detection.

Scheme 1 shows the fabrication of the SPCE/LMA-AgNP/Anti-DD immunosensor step by step.

3. Results and discussion

3.1. Characterization of LMA and LMA-AgNP

The characteristic peaks in the FT-IR spectra for lactose in Fig. 1A were identified and assigned based on comparisons with the literature. The spectrum's bands located between 2925 and 2927 cm^{-1} are indicative of aromatic chemicals or methylene ($-CH_2$). Carbohydrates are linked to bands at 800-1000 cm^{-1}, intermolecular stretching is responsible for a band at 3200 cm^{-1}, and intermolecular stretching is

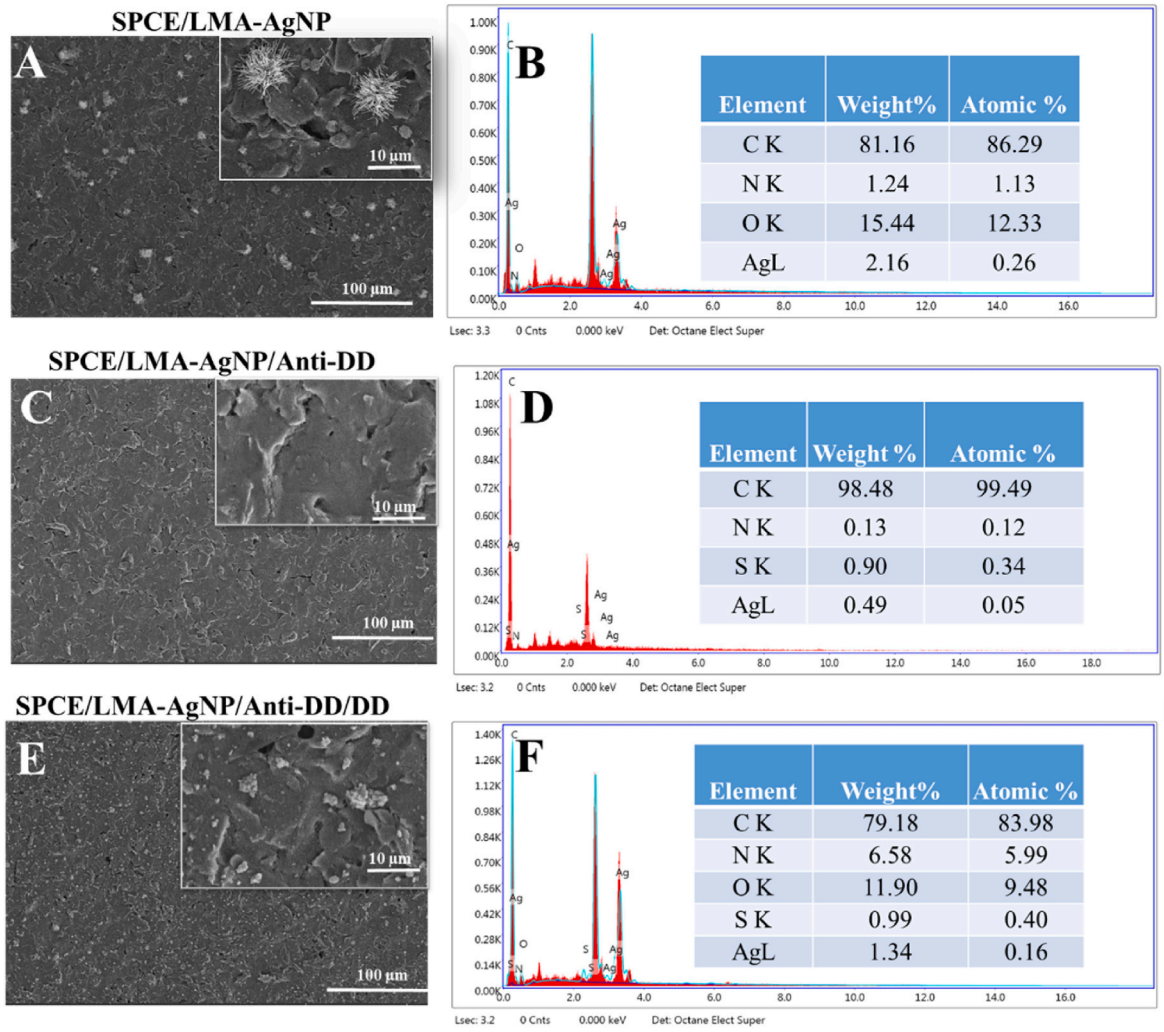

Fig. 2. SEM images of the surface morphology of the electrode modified with (100 µm and inset 10 µm) A) SPCE/LMA-AgNP, C) SPCE/LMA-AgNP/Anti-DD, E) SPCE/LMA-AgNP/Anti-DD/DD. EDS spectrum of B) SPCE/LMA-AgNP D) SPCE/LMA-AgNP/Anti-DD, and F) SPCE/LMA-AgNP/Anti-DD/DD.

responsible for bands at 1150–1030 cm^{-1} [23]. A broad and intense band between 3600 and 3200 cm^{-1} is associated with symmetric -OH stretching. The 1600-1200 cm^{-1} bands were attributed to –CH, -OH, and $–CH_2$ bending vibrations. Glycosidic –C-O-C bending vibrations were observed at 1200-1070 cm^{-1}. The structure of the synthesized LMA is shown in Fig. 1B. The spectra obtained for LMA are presented in Fig. 1C. The broad band observed at 3350 cm^{-1} corresponds to the N-H bond of secondary amines. It is suggested that the peak at 3350 cm^{-1} is attributed to the secondary amine group present in the LMA structure [24]. The 2919 cm^{-1} band attributed to the aromatic C-H stretching [25]. Vibrations between 1250 and 1020 cm^{-1} corresponding to C-N stretching. Additionally, a prominent peak at 1234 cm^{-1} was observed, corresponding to the C-N stretching frequency of 4-methoxy aniline [26]. The region spanning approximately 1040 to 930 cm^{-1} and lower is associated with the stretching vibrations of C-O in the C-OH group, as well as the C-C stretching within the carbohydrate structure [27]. Comparing the peaks obtained from LMA with those of lactose reveals noticeable differences, indicating that lactose has been successfully modified with 4-methoxy aniline. Besides, (+) ESI-MS characterization revealed the synthesis of LMA with a 433.8 *m/z* major peak and a minor peak at 450 *m/z*. It is possible that the applied initial collision energy was high and broke down $-CH_3$, so a major peak was obtained at 433.8 *m/z* as described in the literature [28]. Similarly, the minor peak at 376 *m/z* refers to eliminating methoxy aniline (*m/z* ~123) from the parent molecule (data not shown). Fig. 1D shows the AgNPs are between 650 and 1800 nm size range with snowflake morphology and SPR peak at 560 nm (Fig. 1E). Focusing on the edges of the AgNPs revealed that the smaller particles between ~50 and 160 nm and layers formed the snowflake morphology. This morphology allows for high surface area and increased conductivity [29]. Despite their large size, they were colloidally stable as reported in the literature [30].

3.2. *Characterization of SPCE/LMA-AgNP/Anti-DD immunosensor*

In addition, SEM-EDS analysis was used to look at the topography of the surface. SEM-EDS was used to characterize the structure of the SPCE/LMA-AgNP/Anti-DD immunosensor. EDS analysis was performed to characterize further the SPCE/LMA-AgNP/Anti-DD, specifically the carbon (C), nitrogen (N), oxygen (O), sulfur (S), and silver (Ag) elemental composition were determined at each modification step. SEM images and EDS spectra for the SPCE/LMA-AgNP, SPCE/LMA-AgNP/Anti-DD, and SPCE/LMA-AgNP/Anti-DD/DD shown in Fig. 2 indicate that the surface of the electrodes was differentiated by LMA-AgNP deposition. Fig. 2A shows the electrodeposition of LMA-AgNP on the surface of SPCE. As shown in Fig. 2A, LMA-AgNP is deposited on the surface of SPCE in a crystalline form, and the presence of Ag atoms is confirmed by EDC spectrum analysis (Fig. 2B). After the modification of SPCE/LMA-AgNP with the Anti-DD antibody, SEM image are shown in Fig. 2C, and the S element appeared in the presence of Anti-DD in Fig. 2D. The EDC analysis of SPCE/LMA-AgNP/Anti-DD showed a high

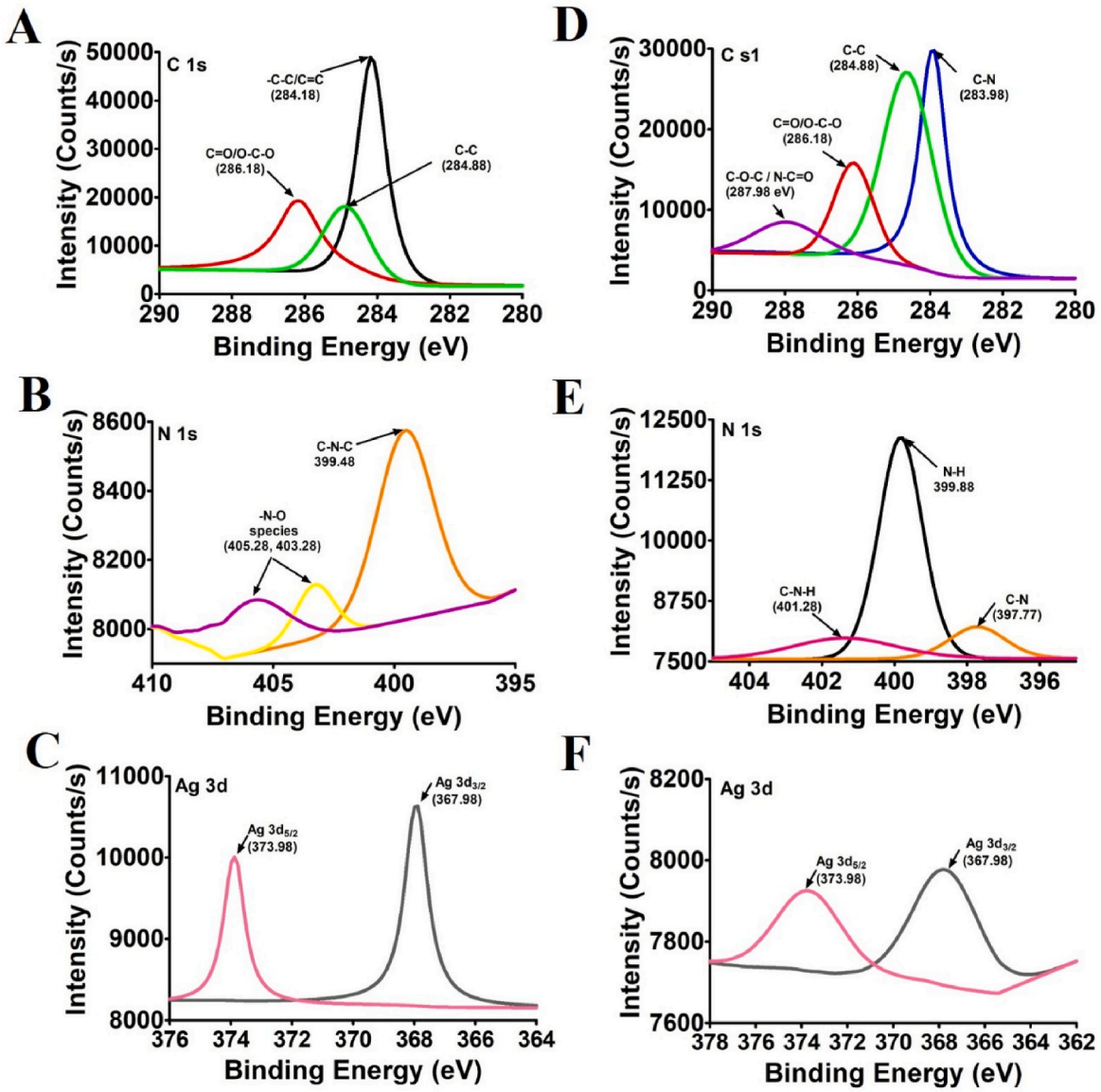

Fig. 3. XPS spectra of A) C 1s B) N 1s C) Ag 3d of SPCE/LMA-AgNP, D) C1s, and E) N 1s and F) Ag 3d of SPCE/LMA-AgNP/Anti-DD and their deconvolutions.

concentration of carbon (99.49 %) with N, S, and Ag (total less than 2 %) as shown in Fig. 2D. As for the SPCE/LMA-AgNP/Anti-DD/DD electrode, the successful development of SPCE/LMA-AgNP/Anti-DD/DD is demonstrated in Fig. 2E by the rise in nitrogen content brought on by the presence of the DD ratio. We have observed the same element present, with a concentration of C 83.98 %, N 5.99 %, S 0.40 % and Ag 0.16 % (Fig. 2F). In all cases, the change in elemental composition indicates that the surface has been successfully modified.

XPS was obtained to confirm valence degrees and surface chemical composition, with the resulting XPS plots presented in Fig. 3A–F. For SPCE/LMA-AgNP in the C 1s spectra (see Fig. 3A), there are three fitted peaks at 286.18 correspond to carbonyl groups of (C=O/O–C–O), while the peak at 284.18 is responsible for –C-C/C=C groups due to LMA structure [31]. The main peak at 284.88 eV is attributed to the C–C of LMA (Fig. 3A) [32]. As for N1s for electrode modified with LMA-AgNP (see Fig. 3B), the peaks at 403.28 eV and 405.68 eV, are attributed to the N–O species of SPCE/LMA-AgNP, corresponding to the 1s to 2b1 and 3π* transitions, respectively [33]. After immobilization of Anti-DD, the C 1s XPS spectrum exhibits four peaks located at 287.98, 286.18, 284.88, and 283.98 eV, which are assigned to C-O-C/N-C=O, C=O/O-C-O, C-C, and C-N, respectively, as shown in Fig. 3D. Also, a binding energy of 399.48 eV was attributed to the presence of pyridinic (C–N–C) [34]. Further, the N 1s spectrum (see Fig. 3E) can be deconvoluted into three peaks corresponding to the terminal amino functions (C-N-H) of LMA-AgNP bond at 401.28 eV, the amine group of LMA (-NH) at 399.88 eV, and 397.78 eV indicate the presence of C–N in Fig. 3D [35–37]. The appearance of the N 1s peak confirms the successful covalent bonding of Anti-DD to the LMA-AgNP modified electrode. Ag NPs are prone to oxidation when exposed to air without adequate protection [38]. However, in Fig. 3C and F, the two peaks at 367.98 eV and 373.98 eV correspond to Ag $3d_3/_2$ and Ag $3d_5/_2$ of metallic Ag NPs, respectively, indicating effective protection of Ag NPs by LMA [18]. It was confirmed that the Ag nanostructures are metallic since no peaks related to AgO (367.4 eV) or Ag_2O (367.8 eV) were seen [39].

3.3. Performance of SPCE/LMA-AgNP/Anti-DD immunosensor

The electrochemical performance of the SPCE/LMA-AgNP/Anti-DD was evaluated using electroanalytical techniques, including CV, DPV, and EIS. Potassium hexacyanoferrate was used as the redox prob. CV and DPV were employed to characterize the modified electrode during each step of the fabrication process, enabling the detection of subtle changes

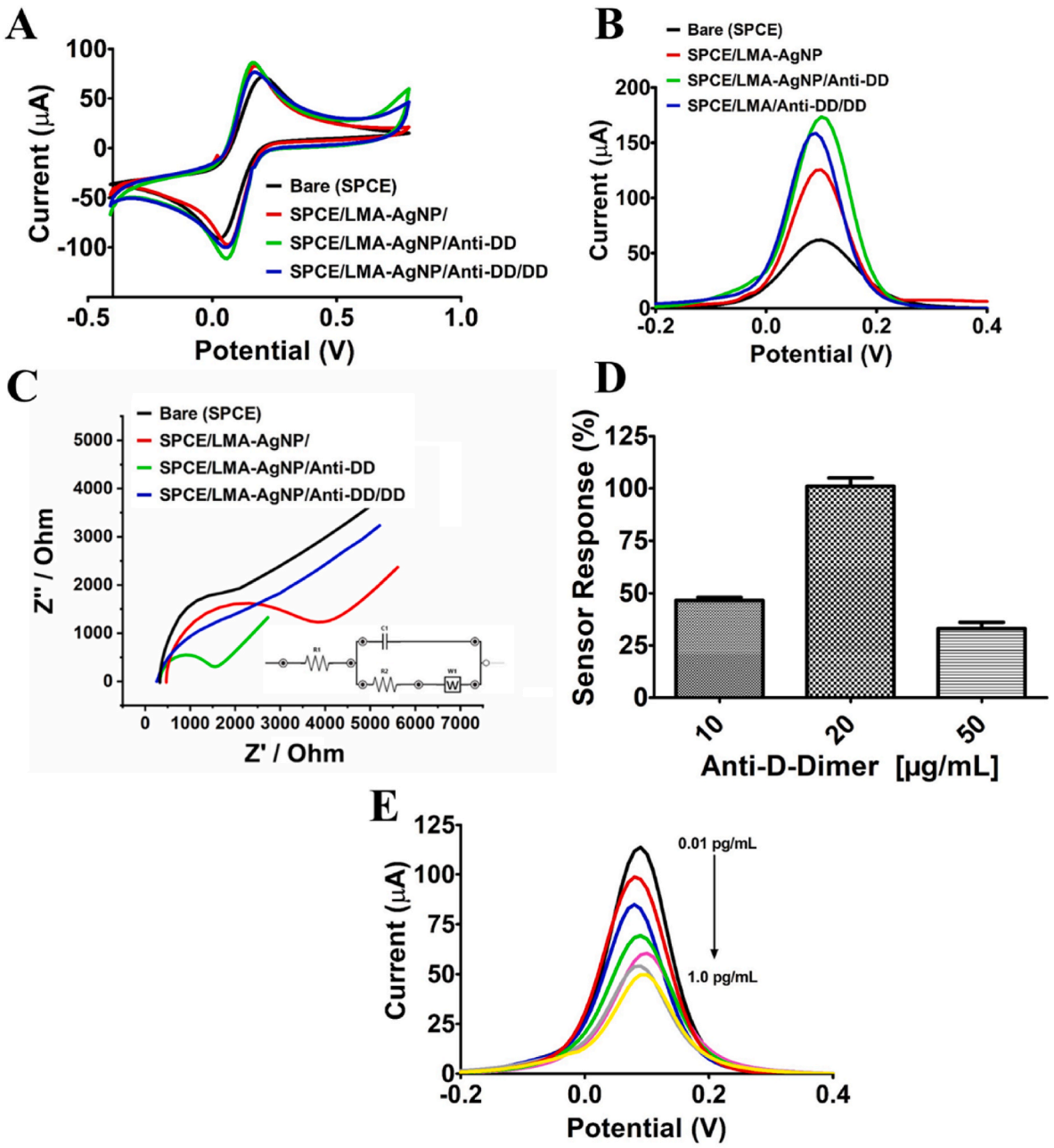

Fig. 4. A) Cyclic voltammogram (CV) B) Differential Pulse Voltammetry (DPV) of Bare SPCE, SPCE/LMA-AgNP, SPCE/LMA-AgNP/Anti-DD and SPCE/LMA-AgNP/Anti-DD/DD with scan rate 50 m/s. C) Nyquist plots for EIS measurement of bare SPCE, SPCE/LMA-AgNP, SPCE/LMA-AgNP/Anti-DD, and SPCE/LMA-AgNP/Anti-DD/DD D) Effect of variety of Anti-DD concentrations on the response of SPCE/LMA-AgNP/Anti-SAA to DD, and E) DPV curves of the electrochemical immunosensor were recorded after incubation with varying concentrations of DD (0.01 pg/mL to 1.0 pg/mL) in a 0.1 M KCl solution containing 5 mM $[Fe(CN)_6]^{3-/4-}$.

between modification stages. According to cyclic voltammograms, I_{anodic} values were found to be 74.34 μA, 81.18 μA, 86.01 μA, and 75.57 μA for bare SPCE, SPCE/LMA-AgNP, SPCE/LMA-AgNP/Anti-DD, and SPCE/LMA-AgNP/Anti-DD/DD, respectively as seen in Fig. 4B. There were peak-to-peak separations of 0.21V for bare SPCE, 0.17 V for SPCE/LMA-AgNP, 0.16 V for SPCE/LMA-AgNP/Anti-DD, and 0.17V for SPCE/LMA-AgNP/Anti-DD/DD measured. The oxidation and reduction peaks of HCF were observed in all CV profiles. Although the current significantly increased after the electrodeposition of LMA-AgNP on SPCE, the current surged again following the immobilization of Anti-DD onto the SPCE/LMA-AgNP. The peak heights increased after immobilizing Anti-DD on the SPCE/LMA-AgNP surface was attributed to electrostatic interactions and the attraction between the $[Fe(CN)_6]^{3-}/[Fe(CN)_6]^{4-}$ couple and the seconder amine due to having structure of LMA onto the SPCE/LMA-AgNP/Anti-DD surface. Similar behavior for amine groups was reported in previous studies, where antibody immobilization increased peak potentials due to interactions with the redox probe [40,41]. A decrease in current was seen in electrochemical tests carried out with DD present as DD attached to the SPCE/LMA-AgNP/Anti-DD electrode surface, resulting in an immunocomplex.

DPV was utilized for quantitative DD detection in this study because it can distinguish peaks even within narrow potential ranges. DPV obtained a similar pattern. According to DPV voltammograms, I_{anodic} values were found to be 61.86, 125.56, 173.43, and 158.64 μA for bare SPCE, SPCE/LMA-AgNP, SPCE/LMA-AgNP/Anti-DD, and SPCE/LMA-AgNP/Anti-DD/DD, respectively as seen in Fig. 4B. In this context, all DPV profiles were consistent with the CV profiles.

The impedance response at each stage of the stepwise electrode

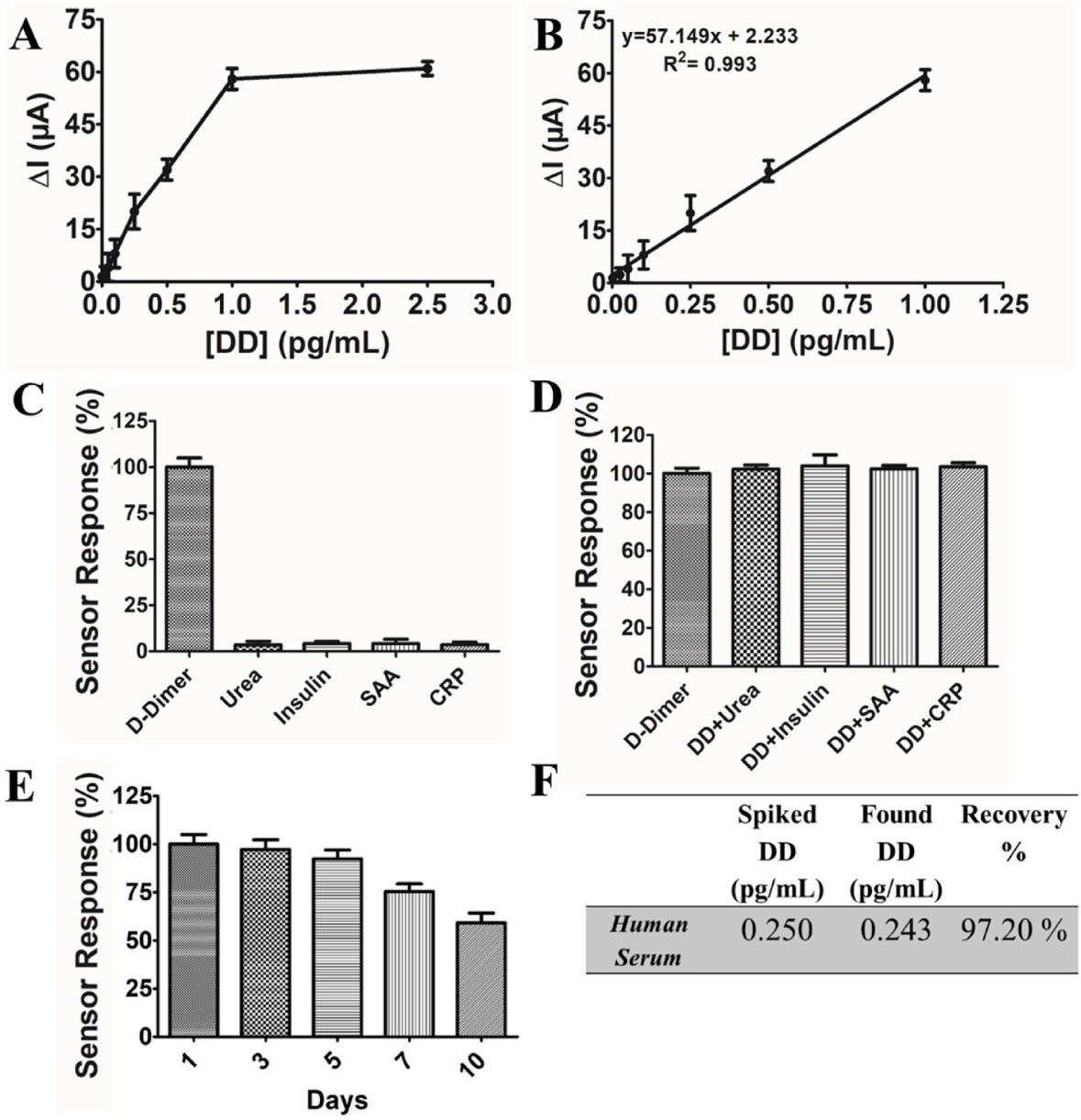

Fig. 5. A) Relationship between DD concentration and sensor response; B) linear range for DD using the SPCE/LMA-AgNP/Anti-DD; C) Substrate specificity of SPCE/LMA-AgNP/Anti-DD; D) Effect of some interfering compounds on SPCE/LMA-AgNP/Anti-DD sensor response to DD (Urea, Insulin, SAA: Serum Amyloid A, CRP: C-Reactive Protein; prepared in PBS pH:7.4; error bars show S.D. of three measurements) E) The stability results of SPCE/LMA-AgNP/Anti-DD (in 5 different days) F) The DD detection in human serum using SPCE/LMA-AgNP/Anti-DD (in the presence of 100 μL of PBS (pH 7.4) solution containing 5 mM HCF and 0.1 M KCl, scan rate: 50 mVs–1, [Anti-DD] = 20 μg/mL).

change is shown in Fig. 4C. The diffusion-limited step of the electrochemical process is represented by a linear zone at low frequencies, while the semicircular region at high frequencies corresponds to the electron transfer-limited process. The charge transfer resistance (Rct), which represents the electrode surface's blocking behavior toward the redox pair, is equal to the semicircle's diameter. As a result, variations in Rct offer important insights about the modification procedure. Randle's equivalent circuit, which incorporates the electrolyte solution resistance (Rs), charge transfer resistance (Rct), constant phase element (CPE), and Warburg impedance (W), is used to describe the biosensor's impedimetric response (inset, Fig. 4C) [42]. As illustrated in Fig. 4C, after electrodeposition, the LMA-AgNP layer on the SPCE electrode had a smaller R_{ct} than Bare SPCE. Reduced Rct is a sign of improved electron transport, facilitated by the well-known conductive properties of AgNPs on the electrode surface. Then immobilization of Anti-DD, a significant decrease in R_{ct} was observed, confirming the successful binding of Anti-DD on SPCE/LMA-AgNP. This decreased R_{ct} can be corresponding to the interaction between the antibody and the negatively charged redox probe [41]. Finally, Rct increased when 1 ng/mL DD was introduced to the SPCE/LMA-AgNP/Anti-DD. The development of a protein layer that obstructs electron transmission is responsible for this rise.

The optimization concentration of Anti-DD was performed using the DPV method. 10, 20, and 50 μg/mL antibody concentrations were used to immobilize Anti-DD on the SPCE/LMA-AgNP. The highest current response, observed in the presence of 1 ng/mL DD, was set as 100 %. The sensor response changes corresponding to different Anti-DD concentrations were calculated and the results are as shown in Fig. 4D. In the presence of DD in a 50 mM PBS solution (pH 7.4), as shown in Fig. 4D, the produced sensor's peak height dropped as a result of the immunocomplex's size, which hindered electron transmission. This behavior is

Table 1
Summarized literature of analytical properties of designed sensor platforms for detection of DD.

Materials	Method	Linear Range	LOD	Ref
AuNPs/DHP	CV,DPV, EIS	1–100 ng/mL	8.92 ng/mL	[44]
AuNpChi	CV, EIS	0–1 μg/mL	$9x10^{-4}$ μg/mL	[9]
Polypyrrole	CV, EIS	0.1–500 ng/mL	100 pg/mL	[47]
SWCNT-COOH	CV, EIS	100 ng/mL-2 μg/mL	0.53 fM	[11]
ZnO	Potentiometric	10^{-6}- 10^{-3} mg/L	100 pg/mL	[48]
SAM	CV, EIS	1–10^3 ng/mL	10 ng/mL	[49]
PEI	CV	0–400 μg/mL	10 ng/mL	[50]
COOH-MBs	Amperometry	0.06–1 μg/mL	0.5 μg/mL	[51]
LMA-AgNP	CV, DPV	0.01–1 pg/mL	0.2 fg/mL	This work

AuNPs: Gold nanoparticles, DHP: di hexadecyl phosphate, Chi: Chitosan, ZnO: Zinc oxide nanorods, SAM: a bifunctional electroactive self-assembled monolayer, PEI: polyethylene imine, COOH-MBs: Carboxylic acid-modified magnetic beads.

consistent with findings in the literature.

DD was detected using DPV within a potential range of −0.2 to +0.4 V in a 5.0 mM $[Fe(CN)_6]^{4-/3-}$ solution. The ΔI of the SPCE/LMA-AgNP/Anti-DD sensor response was calculated before and after incubation with different concentrations of DD. As shown in Fig. 4E, the current (I) decreases with increasing DD concentration due to the accumulation of non-conductive DD molecules on the working electrode surface. The ΔI increases linearly over the 0.01–1.0 pg/mL concentration range, following the equation $y = 57.249x+2.233$ with a correlation coefficient $R^2 = 0.993$ (in Fig. 5A). The formula for LOD is $LOD = 3.3\sigma/S$, where S: is the slope of the calibration curve and σ: sigma is the blank's standard deviation. This yields a value of 0.2 fg/mL. LOD is crucial for the early detection of diseases and monitoring of minimal residual disease, where biomarkers are present in extremely low concentrations. This enables timely intervention and enhances patient outcomes [43]. The antibody sensor demonstrates superior performance for DD detection, characterized by its broad linear range and exceptionally low LOD [44]. For example, Castelnuova et al. showed that DD levels demonstrated a positive correlation with age, were lower in men compared to women, and varied based on smoking status, body mass index, alcohol consumption, and dyslipidemia. Additionally, white blood cell count, lipid profiles, glucose levels, CRP, and diastolic blood pressure all had weak but statistically significant correlations with DD levels [45]. Moreover, Schafer et al. showed findings indicate that venous thromboembolism (VTE), cancer, pneumonia, and other proinflammatory conditions are frequently associated with ultra-high plasma DD levels, even in the absence of a definitive diagnosis. The mortality rate in such patients was significantly elevated, reaching nearly 75 % among those with plasma DD levels exceeding 15 pg/mL. For patients with plasma DD levels above 5 pg/mL and no definitive clinical diagnosis, further diagnostic evaluation is warranted due to the notably high mortality risk in this group [46]. Hence, the developed immunosensor system has the potential to significantly aid clinicians by enabling the rapid and highly sensitive detection of DD at very low concentrations.

Table 1 presents a performance comparison of various electrochemical methods for DD reported in previous studies. The proposed method exhibits superior performance, offering an improved linear range and lower LOD compared to recent literature.

A critical challenge in sensor systems is mitigating the interference effects of other compounds present in the complex matrices of real samples. To evaluate this, selected chemical compounds were introduced into the reaction medium in place of the target, and the resulting signals are shown in Fig. 5C and D. DD levels of 0.50 mg/L or higher may suggest the presence of blood clots within the body. Human SAA and CRP are acute-phase proteins that are elevated during the early stages of inflammation and infection. CRP levels significantly increase in bacterial or mixed infections but show minimal or no elevation in viral infections. In contrast, SAA levels increase in bacterial and viral infections [52]. DD levels are modestly yet significantly correlated with diastolic blood pressure, lipid levels, glucose, CRP, and white blood cell count [45]. Patients with elevated DD levels exhibited higher urea levels than those with lower DD levels [53]. Therefore, we selected urea, insulin, SAA, and CRP as potential interferences of DD to explore the immunossensor's selectivity. The effect on the sensor response of the SPCE/LMA-AgNP/Anti-DD was examined in the presence of some potential interfering compounds and results are indicated in Fig. 5C (in the absence of DD) and in Fig. 5D (in the presence of DD). The SPCE/LMA-AgNP/Anti-DD response was normalized relative to the response at 0.25 pg/mL of DD, which was set as 100 %. According to the results obtained; 1.47 % for urea, 4.24 % for insulin, 4.25 % for SAA, and 3.67 % for CRP were calculated. The responses of the interferences in the presence of DD were calculated as 102.33 % for DD + urea, 104.05 % for DD + Insulin, 102.5 % for DD + SAA, and 103.49 % for DD + CRP. The results indicate that the proposed DD detection assay exhibits high specificity, with no significant interference from potential interferents, as shown in Fig. 5C and D.

The SPCE/LMA-AgNP/Anti-DD remains at approximately 59 % of the initial response to 0.25 pg/mL DD, after a 10-day storage period at 4 °C as illustrated in Fig. 5E. The SPCE/LMA-AgNP/Anti-DD demonstrated high stability for up to 5 days. To evaluate the performance of this SPCE/LMA-AgNP/Anti-DD with real human serum, 0.25 pg/mL of DD was spiked into a human serum sample and analyzed using the SPCE/LMA-AgNP/Anti-DD. As shown in Fig. 5F, the SPCE/LMA-AgNP/Anti-DD successfully detected 97.20 % of the spiked DD, demonstrating acceptable accuracy. Under normal conditions, DD levels are typically low, generally below 0.5 μg/mL fibrinogen equivalent units (FEU) in most clinical assays. However, they increase significantly in patients with thrombosis [54].

4. Conclusions

An immunosensor (SPCE/LMA-AgNP/Anti-DD) was successfully developed for the detection of DD with an excellent detection range. LMA-AgNP was deposited on the SPCE surface and used to conjugate Anti-DD. Compared to a number of well-known electrochemical techniques documented in the literature, the developed SPCE/LMA-AgNP/Anti-DD has a lower LOD and a faster preparation time (Table 1). The designed sensor has a wide analytical range, remarkable sensitivity, and more simplicity than the immunoassays documented in the literature. In addition, the disposable SPCE/LMA-AgNP/Anti-DD detected DD in plasma samples without the need for sample pretreatment. In the future, the developed immunosensor could be easily adapted for inclusion in a ready-to-use commercial kit.

CRediT authorship contribution statement

Fatma Ozturk Kirbay: Writing – review & editing, Writing – original draft, Validation, Resources, Methodology, Investigation, Conceptualization. **İdris Yazgan:** Writing – review & editing, Supervision, Investigation, Data curation. **Dilek Odaci:** Writing – review & editing, Supervision, Resources.

Conflict of interests

The authors declare no conflict of interests.

Acknowledgments

Fatma OZTURK Kırbay thanks to 2218 TUBITAK National Postdoctoral Research Fellowship Program 2021/2 (Project No:121C399). This research was supported by Kastamonu University (Project No: KUBAP-01/2022). The authors thank Dr. Ayşegül Erdoğan at EGE-

MATAL for the XPS analysis.

References

[1] M. Kılıc, O. Yoldas, M. Keskek, T. Ertan, M. Tez, E. Gocmen, M. Koc, Prognostic value of plasma D-dimer levels in patients with colorectal cancer, Color, Dis 10 (2008) 238–241, https://doi.org/10.1111/j.1463-1318.2007.01374.x.

[2] L. Liu, X. Zhang, B. Yan, Q. Gu, X. Zhang, J. Jiao, D. Sun, N. Wang, X. Yue, Elevated plasma D-dimer levels correlate with long term survival of gastric cancer patients, PLoS One 9 (2014) e90547, https://doi.org/10.1371/journal.pone.0090547.

[3] N. Tasić, T.R.L.C. Paixão, L.M. Gonçalves, Biosensing of D-dimer, making the transition from the central hospital laboratory to bedside determination, Talanta 207 (2020) 120270, https://doi.org/10.1016/j.talanta.2019.120270.

[4] A. Lehmann, H. Prosch, S. Zehetmayer, M.R. Gysan, D. Bernitzky, K. Vonbank, M. Idzko, D. Gompelmann, Impact of persistent D-dimer elevation following recovery from COVID-19, PLoS One 16 (2021) e0258351, https://doi.org/10.1371/journal.pone.0258351.

[5] J.L. Elf, K. Strandberg, P.J. Svensson, Performance of two relatively new quantitative D-dimer assays (Innovance D-dimer and AxSYM D-dimer) for the exclusion of deep vein thrombosis, Thromb. Res. 124 (2009) 701–705, https://doi.org/10.1016/j.thromres.2009.07.008.

[6] T.K. Kim, S.W. Oh, Y.J. Mok, E.Y. Choi, Fluorescence immunoassay of human D-dimer in whole blood, J. Clin. Lab. Anal. 28 (2014) 294–300, https://doi.org/10.1002/jcla.21683.

[7] M. Cini, C. Legnani, M. Frascaro, C. Cappelli, M. Sartori, B. Cosmi, Evaluation of a chemiluminescent immunoassay, the HemosIL AcuStar D–Dimer, in outpatients with clinically suspected deep venous thrombosis, Int. J. Lab. Hematol. 37 (2015), https://doi.org/10.1111/ijlh.12420.

[8] M. Pumera, S. Sánchez, I. Ichinose, J. Tang, Electrochemical nanobiosensors, Sensor. Actuator. B Chem. 123 (2007) 1195–1205, https://doi.org/10.1016/j.snb.2006.11.016.

[9] V.C. Rodrigues, M.L. Moraes, J.C. Soares, A.C. Soares, R. Sanfelice, E. Deffune, O. N. Oliveira, Immunosensors made with layer-by-layer films on chitosan/gold nanoparticle matrices to detect d-dimer as biomarker for venous thromboembolism, Bull. Chem. Soc. Jpn. 91 (2018) 891–896, https://doi.org/10.1246/bcsj.20180019.

[10] S. Chebil, N. Macauley, T. Hianik, H. Korri-Youssoufi, Multiwalled carbon nanotubes modified by NTA-copper complex for label-free electrochemical immunosensor detection, Electroanalysis 25 (2013) 636–643, https://doi.org/10.1002/elan.201200298.

[11] S. Bourigua, M. Hnaien, F. Bessueille, F. Lagarde, S. Dzyadevych, A. Maaref, J. Bausells, A. Errachid, N.J. Renault, Impedimetric immunosensor based on SWCNT-COOH modified gold microelectrodes for label-free detection of deep venous thrombosis biomarker, Biosens. Bioelectron. 26 (2010) 1278–1282, https://doi.org/10.1016/j.bios.2010.07.004.

[12] G. Nikoleli, D.P. Nikolelis, N. Tzamtzis, N. Psaroudakis, A selective immunosensor for D-dimer based on antibody immobilized on a graphene electrode with incorporated lipid films, Electroanalysis 26 (2014) 1522–1527, https://doi.org/10.1002/elan.201400161.

[13] A. Abbas, H.M.A. Amin, Silver nanoparticles modified electrodes for electroanalysis: an updated review and a perspective, Microchem. J. 175 (2022) 107166, https://doi.org/10.1016/j.microc.2021.107166.

[14] G. Maduraiveeran, W. Jin, Nanomaterials based electrochemical sensor and biosensor platforms for environmental applications, Trends Environ. Anal. Chem. 13 (2017) 10–23, https://doi.org/10.1016/j.teac.2017.02.001.

[15] I. Yazgan, A. Gümüş, K. Gökkuş, M.A. Demir, S. Evecen, H.A. Sönmez, R.M. Miller, F. Bakar, A. Oral, S. Popov, M.S. Toprak, On the effect of modified carbohydrates on the size and shape of gold and silver nanostructures, Nanomaterials 10 (2020) 1–17, https://doi.org/10.3390/nano10071417.

[16] A. Küçük, Z. Taşdelen, Ş. Güney, S. Sel, E.İ. Demirbaş, F.Ö. Kırbay, S. Sancak, M. Otsus, H.D. Tepe, K. Kasemets, Ç. Kılınç, İ. Yazgan, Development of Inorganic Nanoparticle Glycoconjuate Enhanced Cotton Fabrics for Multi-Drug Resistant Pseudomonas aeruginosa Bacterium, Preprint. (n.d.).

[17] S. Sancak, I. Yazgan, A.U. Bayarslan, A. Ayna, S. Evecen, Z. Taşdelen, A. Gümüş, H. A. Sönmez, M.A. Demir, S. Demir, F. Bakar, H. Dilek-Tepe, K. Kasemets, M. Otsus, T. Çeter, Surface chemistry dependent toxicity of inorganic nanostructure glycoconjugates on bacterial cells and cancer cell lines, J. Drug Deliv. Sci. Technol. 79 (2023) 104054, https://doi.org/10.1016/j.jddst.2022.104054.

[18] I. Yazgan, A. Gümü, S. Popov, M.S. Toprak, On the effect of modified carbohydrates on the size and shape of gold and silver nanostructures, Nanomaterials 10 (2020) 1–17, https://doi.org/10.3390/nano10071417.

[19] M.E. Burgoa Calvo, O. Domínguez Renedo, M.J. Arcos Martínez, Determination of lamotrigine by adsorptive stripping voltammetry using silver nanoparticle-modified carbon screen-printed electrodes, Talanta 74 (2007), https://doi.org/10.1016/j.talanta.2007.05.026.

[20] A. Farahi, M. Achak, L. El Gaini, M.A. El Mhammedi, M. Bakasse, Electrochemical determination of paraquat in citric fruit based on electrodeposition of silver particles onto carbon paste electrode, J. Food Drug Anal. 23 (2015) 463–471, https://doi.org/10.1016/j.jfda.2015.03.003.

[21] M.E. Burgoa Calvo, O. Domínguez Renedo, M.J. Arcos Martínez, Determination of lamotrigine by adsorptive stripping voltammetry using silver nanoparticle-modified carbon screen-printed electrodes, Talanta 74 (2007) 59–64, https://doi.org/10.1016/j.talanta.2007.05.026.

[22] N. Ajermoun, S. Lahrich, A. Farahi, M. Bakasse, S. Saqrane, M.A. El Mhammedi, Electrodeposition of silver onto carbon graphite and their catalysis properties toward thiamethoxam reduction: application in food and beverage samples, Heliyon 6 (2020) e05784, https://doi.org/10.1016/j.heliyon.2020.e05784.

[23] A.L. Balieiro, R.A. Santos, M.M. Pereira, R.T. Figueiredo, L.S. Freitas, O.L.S. de Alsina, A.S. Lima, C.M.F. Soares, Adsorption process of molecularly imprinted silica for extraction of lactose from milk, Brazilian J. Chem. Eng. 33 (2016) 361–372, https://doi.org/10.1590/0104-6632.20160332s20140089.

[24] Identification of sugars and phenolic compounds in honey powders with the use of GC–MS, FTIR Spectroscopy, and X-Ray Diffraction, (n.d.).

[25] D.H. Dawood, M.S. Elmongy, A. Negm, M.A. Taher, Extraction and chemical characterization of novel water-soluble polysaccharides from two palm species and their antioxidant and antitumor activities, Egypt, J. Basic Appl. Sci. 7 (2020) 141–158, https://doi.org/10.1080/2314808x.2020.1773126.

[26] R. Sharma, M.A. Iqubal, S. Jheeta, Kamaluddin, adsorption and oxidation of aromatic amines on metal(II) hexacyanocobaltate(III) complexes: implication for oligomerization of exotic aromatic compounds, Inorganics 5 (2017) 18, https://doi.org/10.3390/inorganics5020018.

[27] S.A. El-Hakam, S.E. Samra, S.M. El-Dafrawy, A.A. Ibrahim, R.S. Salama, A. I. Ahmed, Synthesis of sulfamic acid supported on Cr-MIL-101 as a heterogeneous acid catalyst and efficient adsorbent for methyl orange dye, RSC Adv. 8 (2018) 20517–20533, https://doi.org/10.1039/c8ra02941e.

[28] U. Justesen, Collision-induced fragmentation of deprotonated methoxylated flavonoids, obtained by electrospray ionization mass spectrometry, J. Mass Spectrom. 36 (2001) 169–178, https://doi.org/10.1002/jms.118.

[29] F.A. Khan, C.M. Ajmal, S. Bae, S. Seo, H. Moon, S. Baik, Silver nanoflower decorated graphene oxide sponges for highly sensitive variable stiffness stress sensors, Small 14 (2018) 1–10, https://doi.org/10.1002/smll.201800549.

[30] C.T. Anh, D.T. Cao, L. Truc-Quynh Ngan, Synthesis of colloidal snowflake-like silver nanoparticles and their use for SERS detection of pesticide imidacloprid at trace levels, Opt. Mater. 157 (2024) 116422, https://doi.org/10.1016/j.optmat.2024.116422.

[31] K.L.M. Taaca, M.J.D. De Leon, K. Thumanu, H. Nakajima, N. Chanlek, E.I. Prieto, M.R. Vasquez, Probing the structural features of a plasma-treated chitosan-acrylic acid hydrogel, Colloids Surfaces A Physicochem. Eng. Asp. 637 (2022) 128233, https://doi.org/10.1016/j.colsurfa.2021.128233.

[32] C. I.P, R. S, Characterization of a new natural cellulosic fiber extracted from Derris scandens stem, Int. J. Biol. Macromol. 165 (2020) 2303–2313, https://doi.org/10.1016/j.ijbiomac.2020.10.086.

[33] C.W. Zou, X.D. Yan, J. Han, R.Q. Chen, W. Gao, J. Metson, Study of a nitrogen-doped ZnO film with synchrotron radiation, Appl. Phys. Lett. 94 (2009), https://doi.org/10.1063/1.3125255.

[34] S. Chandra, D. Bano, P. Pradhan, V.K. Singh, P.K. Yadav, D. Sinha, S.H. Hasan, Nitrogen/sulfur-co-doped carbon quantum dots: a biocompatible material for the selective detection of picric acid in aqueous solution and living cells, Anal. Bioanal. Chem. 412 (2020) 3753–3763, https://doi.org/10.1007/s00216-020-02629-1.

[35] L. Ge, F. Zuo, J. Liu, Q. Ma, C. Wang, D. Sun, L. Bartels, P. Feng, Synthesis and efficient visible light photocatalytic hydrogen evolution of polymeric g-C_3N_4 coupled with CdS quantum dots, J. Phys. Chem. C 116 (2012) 13708–13714, https://doi.org/10.1021/jp3041692.

[36] Z. Li, D. Li, F. Yu, L. Dong, L. Zang, J. Zhang, L. Shi, X. Ge, S. Guo, Y. Zheng, Novel 2D photocatalyst of copper-doped carbon quantum dot CD(Cu) loaded with ultrathin Ni-MOL for degradation of tetracycline, Water Sci. Technol. 86 (2022) 1835–1847, https://doi.org/10.2166/wst.2022.306.

[37] A. Meena, C. Bathula, M.R. Hatshan, R.R. Palem, A. Jana, Microstructure and oxygen evolution property of prussian blue analogs prepared by mechanical grinding, Nanomaterials 13 (2023) 2459, https://doi.org/10.3390/nano13172459.

[38] G. Zhang, Y. Xiao, Q. Yin, J. Yan, C. Zang, H. Zhang, In situ synthesis of silver nanoparticles on amino-grafted polyacrylonitrile fiber and its antibacterial activity, Nanoscale Res. Lett. 16 (2021) 36, https://doi.org/10.1186/s11671-021-03496-0.

[39] J. Feng, D. Fan, Q. Wang, L. Ma, W. Wei, J. Xie, J. Zhu, Facile synthesis silver nanoparticles on different xerogel supports as highly efficient catalysts for the reduction of p-nitrophenol, Colloids Surfaces A Physicochem. Eng. Asp. 520 (2017) 743–756, https://doi.org/10.1016/j.colsurfa.2017.02.041.

[40] S. Sanli, Single-drop electrochemical immunosensor with 3D-printed magnetic attachment for onsite smartphone detection of amoxicillin in raw milk, Food Chem. 437 (2024) 137823, https://doi.org/10.1016/j.foodchem.2023.137823.

[41] F. Ozturk Kirbay, D. Odaci, Electrospun poly-ε-caprolactone/poly-l-lysine (PCL/PLL) nanofibers as an emergent material for the preparation of electrochemical immunosensor to detect serum amyloid A, ACS Appl. Polym. Mater. 6 (2024) 3778–3786, https://doi.org/10.1021/acsapm.3c03002.

[42] E.B. Aydın, Highly sensitive impedimetric immunosensor for determination of interleukin 6 as a cancer biomarker by using conjugated polymer containing epoxy side groups modified disposable ITO electrode, Talanta 215 (2020) 120909, https://doi.org/10.1016/j.talanta.2020.120909.

[43] H. Moulahoum, F. Ghorbanizamani, The LOD paradox: when lower isn't always better in biosensor research and development, Biosens. Bioelectron. 264 (2024) 116670, https://doi.org/10.1016/j.bios.2024.116670.

[44] N. Tasić, L. Cavalcante, E. Deffune, M.S. Góes, T.R.L.C. Paixão, L.M. Gonçalves, Probeless and label-free impedimetric biosensing of D-dimer using gold nanoparticles conjugated with dihexadecylphosphate on screen-printed carbon electrodes, Electrochim. Acta 397 (2021), https://doi.org/10.1016/j.electacta.2021.139244.

[45] A. Di Castelnuovo, A. de Curtis, S. Costanzo, M. Persichillo, M. Olivieri, F. Zito, M. B. Donati, G. de Gaetano, L. Iacoviello, Association of D-dimer levels with all-cause mortality in a healthy adult population: findings from the MOLI-SANI study,

Haematologica 98 (2013) 1476–1480, https://doi.org/10.3324/haematol.2012.083410.
[46] K. Schafer, E. Goldschmidt, D. Oostra, J. Fish, T. Russell, F. Lurie, The clinical significance of ultra-high D-dimer levels, J. Vasc. Surg. Venous Lymphat. Disord. 10 (2022) 8–13, https://doi.org/10.1016/j.jvsv.2021.06.011.
[47] S. Chebil, I. Hafaiedh, H. Sauriat-Dorizon, N. Jaffrezic-Renault, A. Errachid, Z. Ali, H. Korri-Youssoufi, Electrochemical detection of d-dimer as deep vein thrombosis marker using single-chain d-dimer antibody immobilized on functionalized polypyrrole, Biosens. Bioelectron. 26 (2010) 736–742, https://doi.org/10.1016/j.bios.2010.06.048.
[48] Z.H. Ibupoto, N. Mitrou, G. Nikoleli, D.P. Nikolelis, M. Willander, N. Psaroudakis, The development of highly sensitive and selective immunosensor based on antibody immobilized ZnO nanorods for the detection of D-dimer, Electroanalysis 26 (2014) 292–298, https://doi.org/10.1002/elan.201300580.
[49] S.M. Marques, A. Santos, L.M. Gonçalves, J.C. Sousa, P.R. Bueno, Sensitive label-free electron chemical capacitive signal transduction for D-dimer electroanalysis, Electrochim. Acta 182 (2015) 946–952, https://doi.org/10.1016/j.electacta.2015.09.169.
[50] A.L.Y. Yokomichi, V. da C. Rodrigues, A. Moroz, M. Bertanha, S.J.L. Ribeiro, E. Deffune, M.L. Moraes, Detection of factor VIII and D-dimer biomarkers for venous thromboembolism diagnosis using electrochemistry immunosensor, Talanta 219 (2020) 121241, https://doi.org/10.1016/j.talanta.2020.121241.
[51] M. Gamella, S. Campuzano, F. Conzuelo, A.J. Reviejo, J.M. Pingarrón, Amperometric magnetoimmunosensors for direct determination of D-dimer in human serum, Electroanalysis 24 (2012) 2235–2243, https://doi.org/10.1002/elan.201200503.
[52] N.M. Frame, M. Kumanan, T.E. Wales, A. Bandara, M. Fändrich, J.E. Straub, J. R. Engen, O. Gursky, Structural basis for lipid binding and function by an evolutionarily conserved protein, serum amyloid A, J. Mol. Biol. 432 (2020) 1978–1995, https://doi.org/10.1016/j.jmb.2020.01.029.
[53] C.P. Domingueti, R.B. Fóscolo, L.M.S. Dusse, J.S. Reis, M. das G. Carvalho, K. B. Gomes, A.P. Fernandes, Association of different biomarkers of renal function with D-dimer levels in patients with type 1 diabetes mellitus (renal biomarkers and D-dimer in diabetes), Arch. Endocrinol. Metab. 62 (2018) 27–33, https://doi.org/10.20945/2359-3997000000003.
[54] E.D. Johnson, J.C. Schell, G.M. Rodgers, The D-dimer assay, Am. J. Hematol. 94 (2019) 833–839, https://doi.org/10.1002/ajh.25482.